Current Biology 21, 1918–1923, November 22, 2011 ©2011 Elsevier Ltd All rights reserved DOI 10.1016/j.cub.2011.10.002

Report

Positional Information by Differential Endocytosis Splits Auxin Response to Drive *Arabidopsis* Root Meristem Growth

Luca Santuari,[1,4] Emanuele Scacchi,[1,4] Antia Rodriguez-Villalon,[1] Paula Salinas,[1] Esther M.N. Dohmann,[1] Géraldine Brunoud,[2] Teva Vernoux,[2] Richard S. Smith,[3] and Christian S. Hardtke[1,*]

[1]Department of Plant Molecular Biology, University of Lausanne, Biophore Building, CH-1015 Lausanne, Switzerland

[2]Laboratoire de Reproduction et Développement des Plantes, CNRS, INRA, ENS Lyon, UCBL, Université de Lyon, 69364 Lyon, France

[3]Institute of Plant Sciences, University of Bern, Altenbergrain 21, Bern CH-3013, Switzerland

Summary

In the *Arabidopsis* root meristem, polar auxin transport creates a transcriptional auxin response gradient that peaks at the stem cell niche and gradually decreases as stem cell daughters divide and differentiate [1–3]. The amplitude and extent of this gradient are essential for both stem cell maintenance and root meristem growth [4, 5]. To investigate why expression of some auxin-responsive genes, such as the essential root meristem growth regulator *BREVIS RADIX* (*BRX*) [6], deviates from this gradient, we combined experimental and computational approaches. We created cellular-level root meristem models that accurately reproduce distribution of nuclear auxin activity and allow dynamic modeling of regulatory processes to guide experimentation. Expression profiles deviating from the auxin gradient could only be modeled after intersection of auxin activity with the observed differential endocytosis pattern and positive autoregulatory feedback through plasma-membrane-to-nucleus transfer of BRX. Because BRX is required for expression of certain auxin response factor targets, our data suggest a cell-type-specific endocytosis-dependent input into transcriptional auxin perception. This input sustains expression of a subset of auxin-responsive genes across the root meristem's division and transition zones and is essential for meristem growth. Thus, the endocytosis pattern provides specific positional information to modulate auxin response.

Results and Discussion

Differential distribution of auxin by polar auxin transport (PAT) regulates cellular characteristics such as proliferation, elongation, and differentiation and depends on nonuniform (polar) plasma membrane localization of PIN-FORMED (PIN) auxin efflux carriers [1]. Along the root meristem, PAT creates an auxin response gradient, which peaks at the stem cell niche and decreases as stem cell daughters proliferate in the meristematic zone [2, 3]. Their eventual differentiation and elongation are timed by complex dynamic hormone pathway crosstalk in the so-called transition zone, which creates a developmental window in young roots to permit meristem growth [4–6]. The *BREVIS RADIX* (*BRX*) gene is essential for this process and is expressed in developing vasculature, mainly in the protophloem [6, 7]. In *brx* mutants, suspended meristem growth coincides with diminished auxin response as BRX limits auxin-responsive transcription, likely through modulation of auxin response factor (ARF) activity and downstream effects on brassinosteroid levels [6, 7]. Interestingly, *BRX* is itself auxin responsive and targeted by the ARF MONOPTEROS (MP). Paradoxically, however, the expression profile of *BRX* as well as other MP targets does not always follow the described auxin response gradient across the meristematic and transition zones [6] (Figure 1A). In this study, we combined experimental and modeling approaches to investigate this phenomenon.

In a first step, we created a cellular-level *Arabidopsis* root-meristem model, centered across the two protophloems, where *BRX* expression is most prominent and robust. Throughout our study, confocal microscopy allowed unequivocal identification of the protophloem strands as a result of their unique cell wall staining characteristics after modified pseudo-Schiff propidium iodide and/or propidium iodide staining [6, 8] and because of their distinct morphology as compared to the xylem strands (see Figure S1A available online). Because the phloem poles are not planar, a slightly curved plane through a serial stack of confocal sections was extracted using a Bézier surface. Its segmentation rendered a two-dimensional model of cellular structure (Figure 1B), from which an idealized variant was derived (Figure 1C) (see Supplemental Experimental Procedures for model details). The model's PAT topography after incorporation of the previously reported PIN distribution [9] dynamically recreated the stem cell niche auxin maximum and gradient once steady state was reached after feeding auxin through the vasculature (Figure 1C; Movie S1A). However, modeled cellular auxin concentration gradually increased toward the elongation zone, a feature that had not been observed previously [9]. Gradually increased auxin concentration toward the elongation zone was also not observed in auxin measurements [2]; however, because the modeled relative increase is comparatively small, this could reflect the limited cellular and technical resolution of this approach. Recreation of a grid model similar to Grieneisen et al. [9] reproduced this feature if the parameter of the ratio between passive and active (PIN-mediated) auxin transport was adjusted (Figure S1B). To obtain a clearer picture of auxin activity across the meristem, we estimated it in vivo using the constitutively expressed fluorescent DII-VENUS reporter [10]. DII-VENUS is degraded upon auxin-triggered interaction with nuclear auxin receptors [11–13], which are ubiquitously expressed throughout the root [14]. DII-VENUS abundance thus correlates inversely with cellular auxin activity and should reflect auxin concentration. Interestingly, experimentally observed DII-VENUS fluorescence intensity matched with our modeled auxin distribution pattern. An exception was the protophloem (and the protoxylem, which was however not considered separately in our model), where relative to neighboring tissue layers, increased auxin activity was indicated (Figures 1D and 1E; Figure S1C). This experimental finding could be re-created by addition of the protophloem-specific auxin influx

[4]These authors contributed equally to this work
*Correspondence: christian.hardtke@unil.ch

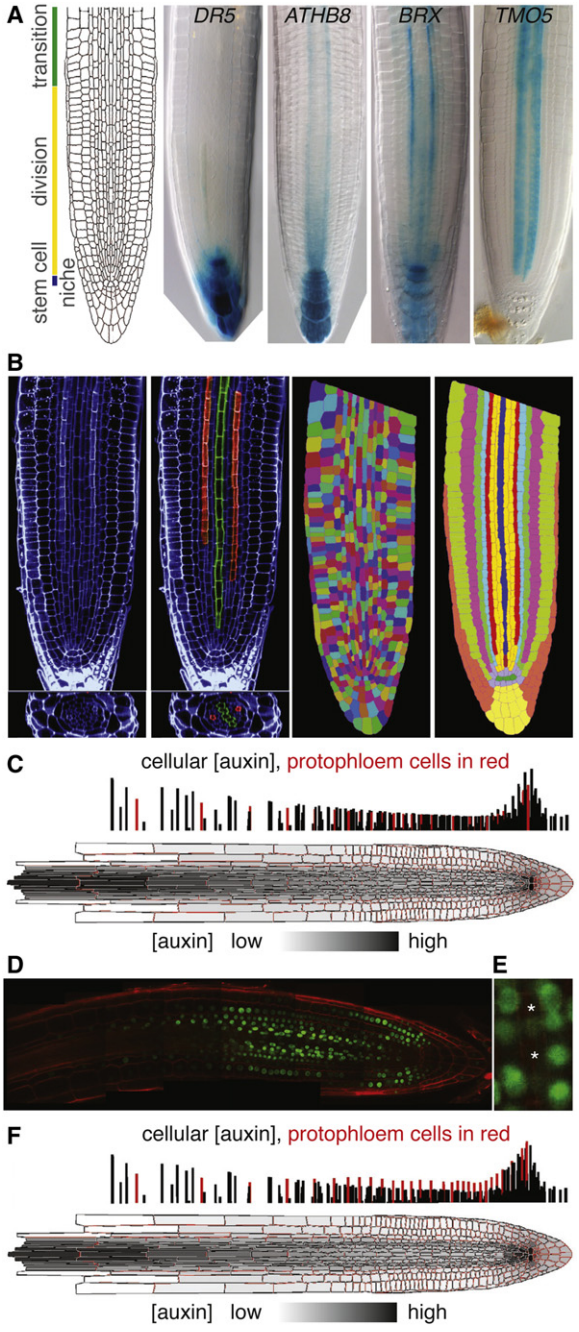

Figure 1. A Cellular-Level *Arabidopsis* Root Meristem Model

(A) Schematic presentation of different meristem regions and staining patterns of GUS reporters driven by promoters of the *DR5* auxin response marker and auxin-responsive genes *ATHB8*, *BRX*, and *TMO5*.

(B) Modeling illustration. Marking bilateral symmetry in serial confocal section stacks of a 3-day-old modified pseudo-Schiff propidium iodide-stained root meristem (protophloem in red; protoxylem in green) allowed extraction of a curved section using a Bézier surface. Subsequent segmentation rendered a 2D model of cellular structure that was tissue-type coded.

(C) Modeled steady-state auxin distribution after implementation of experimentally observed PIN auxin efflux carriers [9] and apical auxin feeding through the vasculature (bottom). Bars represent the relative auxin content of individual cells in a 2D projection (top). Cellular auxin activity is considered as a direct function of auxin concentration.

(D) Distribution of constitutively expressed DII-VENUS auxin activity reporter in the root meristem, visualized by two-photon microscopy across the protophloem poles.

carrier AUXIN RESISTANT 1 (AUX1) [15] (Figure 1F). Alternatively, the same effect could be obtained by increased bulk flow of auxin through the phloem, a phenomenon that is particularly prominent at later stages of seedling development, from 5 days after germination (dag) onward [16]. However, we did not consider this option because our model focused on undifferentiated cells and the earlier stage of root meristem growth at 3 dag. The model was robust across a parameter range and re-created the experimentally observed auxin activity distribution landscape at cellular resolution (Movie S1B). The only tissue where we found significant variation in relative DII-VENUS intensity between individual samples was the epidermis. This appeared to result from root bending consistent with differential lateral auxin fluxes due to gravitropism [17]. Notably, increasing epidermal auxin retention uni- or bilaterally through modulating lateral inward PIN abundance did not alter the relative auxin activity profile of the vascular tissue layers (Movies S3B and S3C). Thus, we kept relative auxin in the epidermis low in follow-up models, for better viewing of results but also consistent with a straight root and epidermal auxin measurements [2].

Confirming the initial paradox, auxin activity distribution only partially matched the *BRX* transcription profile (Figure 2A), suggesting a significant influence of other factors. To determine which conditions could create this profile, we added *BRX* transcription and the established regulatory influences that modulate it to our model. This included response to cellular auxin concentration, but also positive autoregulatory *BRX* feedback, which is required for maintenance of its own expression level and continuity [7] (Figure 2B). As could be expected, this dynamic model produced a *BRX* steady-state expression profile that followed auxin activity distribution, suggesting that additional factors must play a role. One important factor could be differential plasma membrane versus nuclear partitioning of BRX protein. Various experimental evidences suggest that BRX is a transcriptional coregulator; however, BRX is primarily plasma membrane associated [18, 19]. Passage by the plasma membrane appears to be obligatory for its nuclear activity, because BRX variants with disrupted plasma membrane targeting (either by N-terminal extension or by mutation of a nuclear export signal into a nuclear localization signal) could not rescue the *brx* mutant (Figure 2C). Thus, position-dependent plasma-membrane-to-nucleus trafficking of BRX could introduce an asymmetry to its autoregulatory feedback. Plasma membrane abundance of constitutively expressed BRX-GFP fusion protein indeed varies along the developing protophloem and is accompanied by a corresponding gradient of nuclear activity [6]. When this position-dependent plasma-membrane-to-nucleus transfer rate was implemented, the modeled *BRX* expression profile approached the experimental one (Figure 2E; Movie S2A).

In our attempt to refine the model and transform BRX plasma membrane abundance into a dynamic parameter, documented endocytic recycling of BRX was of particular interest, because BRX nuclear import is trafficking dependent [19]. Pharmacological inhibition of BRX endocytosis by tyrphostin A23 treatment as well as coimmunoprecipitation of clathrin heavy chain suggests that endocytic recycling of BRX uses the clathrin-mediated pathway (Figure 2F; Figure 3A) [20].

(E) Decreased DII-VENUS abundance in the nuclei of protophloem cells (next to asterisks) as compared to neighboring tissue layers.

(F) Modeled steady-state auxin distribution after model extension by implementation of the auxin influx carrier AUX1.

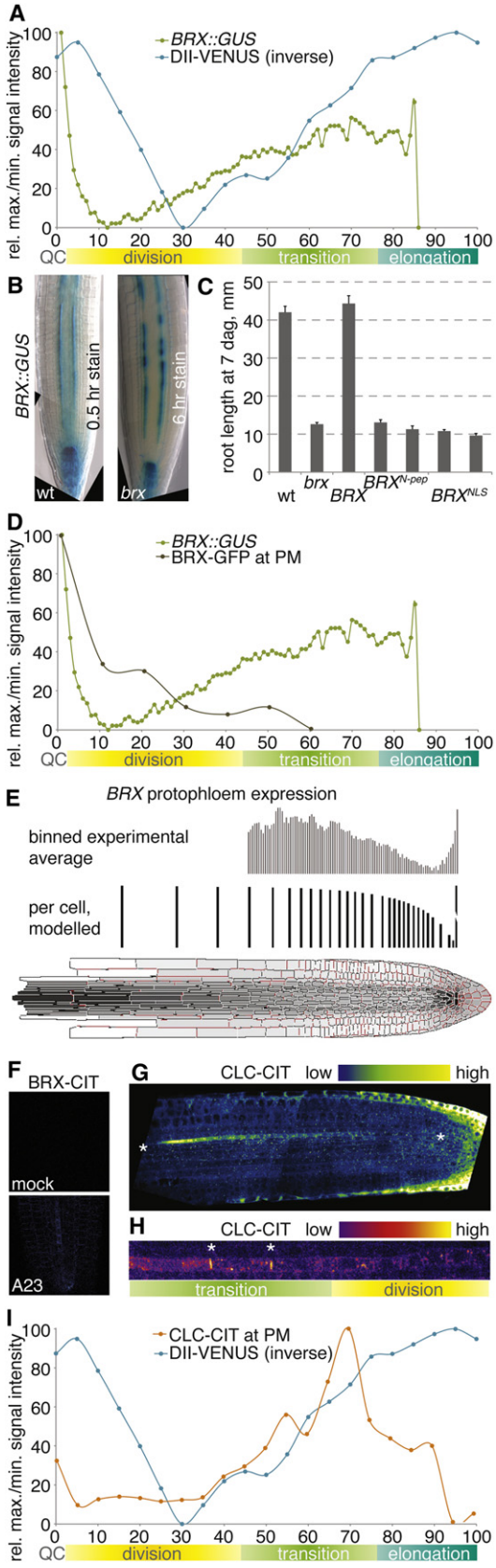

Figure 2. Relation between BRX Autoregulatory Feedback and Endocytosis

(A) Experimental vascular profiles of relative auxin activity (DII-VENUS) and *BRX* expression (*BRX::GUS*) from the quiescent center (QC) toward the elongation zone (displayed values are averages; n = 6 and 18, respectively; average standard error for both curves < 1%).

(B) *BRX::GUS* expression in wild-type (wt) and *brx* mutant (*brx*). Note the longer staining and patchiness of expression in the *brx* background.

(C) Propensity of constitutively expressed *BRX* and variants with disturbed plasma membrane targeting ($BRX^{N\text{-}pep}$, BRX^{NLS}) to rescue the *brx* root growth defect (displayed values are averages; n = 12). Error bars indicate standard errors.

(D) Experimental profiles of *BRX* expression (*BRX::GUS*) and plasma membrane abundance of constitutively expressed BRX-GFP (displayed values are averages; n = 18 and 13, respectively; average standard error < 1% and < 3%, respectively) along the protophloem.

(E) Experimentally observed and dynamically modeled *BRX* expression profiles after model extension by incorporating auxin control of *BRX* and differential BRX autoregulatory feedback due to position-dependent plasma membrane versus nuclear partitioning.

(F) Plasma membrane accumulation of constitutively expressed BRX-CITRINE (BRX-CIT) 45 min after blocking endocytosis by A23 treatment (30 μM) as compared to mock.

(G) Differential plasma membrane accumulation of constitutively expressed clathrin light chain-CITRINE (CLC-CIT) in the root meristem visualized by two-photon microscopy (color-coded heat map). Note the high activity in the protophloem file (indicated by asterisks).

(H) Increasing plasma membrane accumulation of CLC-CIT along the protophloem visualized by two-photon microscopy (color-coded heat map). Note polar localization (asterisks).

(I) Experimental vascular profiles of auxin concentration (DII-VENUS) and CLC-CIT polar plasma membrane recruitment (displayed values are averages; n = 6 and 7, respectively; average standard error < 1% and < 7%, respectively).

The latter can be inhibited by auxin [21], which could thus be responsible for differential BRX plasma membrane abundance. The correlation with observed auxin activity was limited, however, as underlined by strong local discrepancies, notably in the quiescent center and the meristematic and transition zones (compare Figures 2A and 2D). To estimate the degree of clathrin-mediated endocytosis in the developmental context of the root meristem, we monitored a constitutively expressed fusion protein of clathrin light chain and fluorescent CITRINE (CLC-CIT). Surprisingly, CLC-CIT plasma membrane accumulation, which indicates endocytosis activity [20, 21], varied considerably between root meristem cells in a pattern that overall did not match the expectation from auxin activity distribution (Figure 2G). For example, in the meristematic and transition zones, highest endocytosis activity was observed in developing protophloem (Figure 2H), unexpectedly concomitant with relatively higher auxin activity (Figure 2I). Also, endocytosis appeared to be particularly active in the quiescent center, the location of highest auxin levels [2, 9]. This pattern suggests that there may be no simple inverse correlation between endocytic activity and auxin concentration, with the caveat that it is unknown whether intra- and extracellular auxin levels correspond perfectly [22]. Unless a reliable method to determine apoplastic auxin concentration in situ is found, this question cannot be resolved. The profiles of modeled intra- and extracellular auxin based on observed PIN abundance are very similar [9]. This was also true once our parameters were implemented in the grid model (Figure S1D), which is the reason why we did not explicitly model the apoplast. When our model was extended by auxin inhibition of endocytosis, this resulted in BRX internalization as early as in the early meristematic zone and rapid upregulation of *BRX* expression close to the quiescent center (Movie S2B). By contrast, endocytosis activity matched decreasing BRX plasma membrane abundance and increasing *BRX* expression (compare Figures 2D and 2I). Moreover, CLC-CIT displayed polarized plasma membrane association in protophloem

A

protein	unique peptides	peptide count in IP BRX-GFP	PM-GFP
heavy clathrin chain At3g08530	23	23	10
heavy clathrin chain At3g11130	2	2	0

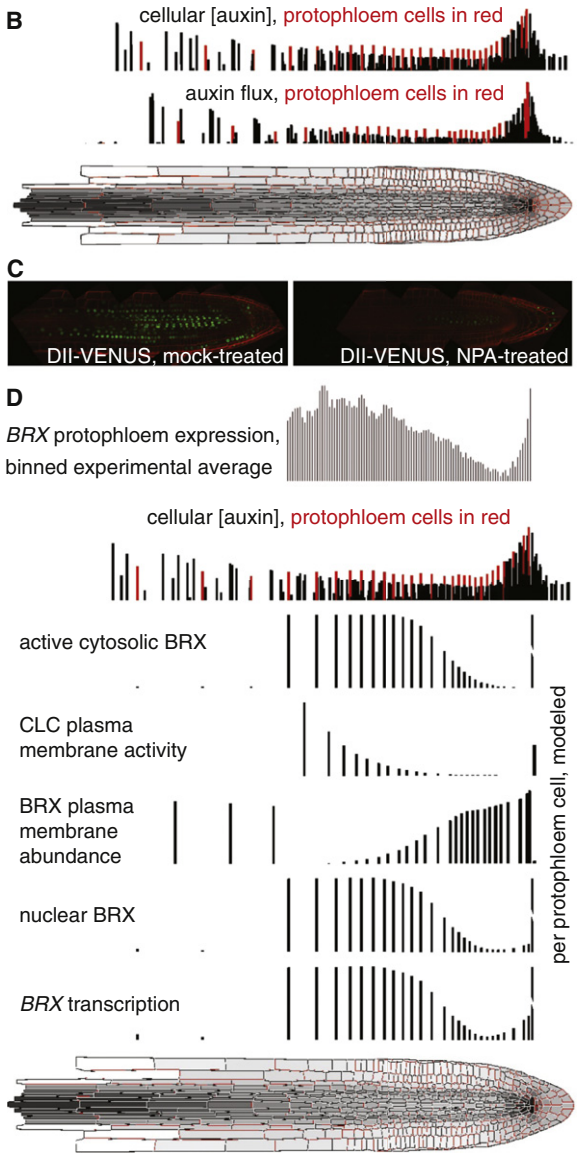

Figure 3. Endocytosis-Based Model of BRX Autoregulatory Feedback

(A) Enrichment of clathrin heavy chain peptides as determined by MALDI-TOF mass spectrometry after immunoprecipitation of BRX-GFP (control: plasma membrane-associated GFP [PM-GFP] [25]).

(B) Profiles of modeled steady-state levels of auxin concentration and flux.

(C) Disappearance of constitutively expressed DII-VENUS upon polar auxin transport inhibition by naphthylphthalamic acid (NPA) treatment (5 μM, 16 hr).

(D) Modeled steady-state profiles in the refined model after incorporation of BRX autoregulatory feedback as a function of differential endocytosis.

(Figure 2H), similar to BRX [19], and both endocytosis activity and *BRX* expression decreased at the end of the transition zone. This is consistent with a dominant role of endocytosis for *BRX* autoregulatory feedback, which would also explain why meristematic *BRX* expression is mainly confined to protophloem.

We also sought to take into account that BRX plasma membrane dissociation can be transiently induced by auxin treatment [19], which we confirmed biochemically (Figure S1E). Because blocking exocytosis of internalized BRX by brefeldin A treatment has the same effect [19], the rate of endocytic recycling might determine the equilibrium between BRX plasma membrane redelivery and nuclear transfer. Consistent with this idea, BRX nuclear transfer could not be induced by auxin in cells with a low endocytosis rate as judged from CLC-CIT accumulation, i.e., in meristematic cells other than protophloem as opposed to differentiated cells [19]. The alternative idea that BRX localization could depend on auxin flux, suggested by increased BRX plasma membrane abundance upon PAT inhibition [19], could not be verified, because auxin concentration and flux correlated closely in our model (Figure 3B). Rather, similar PAT inhibition led to increased cellular auxin concentration (Figure 3C), thereby corroborating the inhibitory effect of high auxin on endocytosis. We thus conclude that auxin must primarily act on the nuclear transfer of internalized BRX, which was included in our model. In summary, our results point to a possibly dosage-dependent and bimodal auxin impact on endocytosis, where higher concentrations inhibit and lower concentrations permit or even promote endocytosis. However, such considerations could not dynamically link auxin and endocytosis activity in our model, suggesting that other, unknown factors could play an important role in setting up the endocytosis pattern. It also appears possible that there is low auxin in the apoplast of cells with high auxin uptake capacity (for instance, because of AUX1 activity) and thus high cellular auxin concentration. It is impossible at the moment to verify the degree to which apoplastic auxin determines the endocytosis pattern because of the technical limit of apoplastic auxin detection, but this might be a promising subject for modelers of auxin transport. Irrespective of these considerations, however, incorporating the endocytosis pattern into our model as a conditioner of auxin effects on BRX dynamically recreated the *BRX* expression profile (Figure 3D; Movie S3A), not only in the longitudinal dimension but also across the phloem axis.

Because the *DR5::GUS* reporter, whose promoter consists of multimerized ARF binding sites and therefore monitors overall ARF activity [3], is underexpressed in *brx* mutants, a prediction of our model was that its expression should be partly endocytosis dependent. Tyrphostin A23 treatment indeed affected *DR5::GUS* expression where endocytosis was active and *BRX* was expressed, notably around the quiescent center (Figure 4A). Moreover, activation of *DR5::GUS* expression by auxin induction was drastically diminished in the presence of tyrphostin A23, in particular in the transition zone (Figure 4B). To determine whether endocytosis, through BRX, affects individual auxin-response genes in a generic or specific manner, we monitored reporter gene expression of experimentally confirmed ARF targets, *ARABIDOPSIS THALIANA HOMEOBOX 8* (*ATHB8*), *TARGET OF MONOPTEROS 5* (*TMO5*), and *TMO7* [23, 24], in a *brx* mutant background. Interestingly, whereas *ATHB8* and *TMO7* were not visibly affected (Figure 4C-D), *TMO5* expression was strongly reduced specifically in the meristematic and transition zones of *brx* meristems (Figure 4E). Because *TMO5* is mainly expressed in developing xylem in the meristematic zone (Figures 4F–4H), this might in part reflect previously described non-cell-autonomous action of *BRX* [6]. However, it could also be due to direct regulation, because low levels of *BRX* expression have been observed in meristematic protoxylem [6], and because

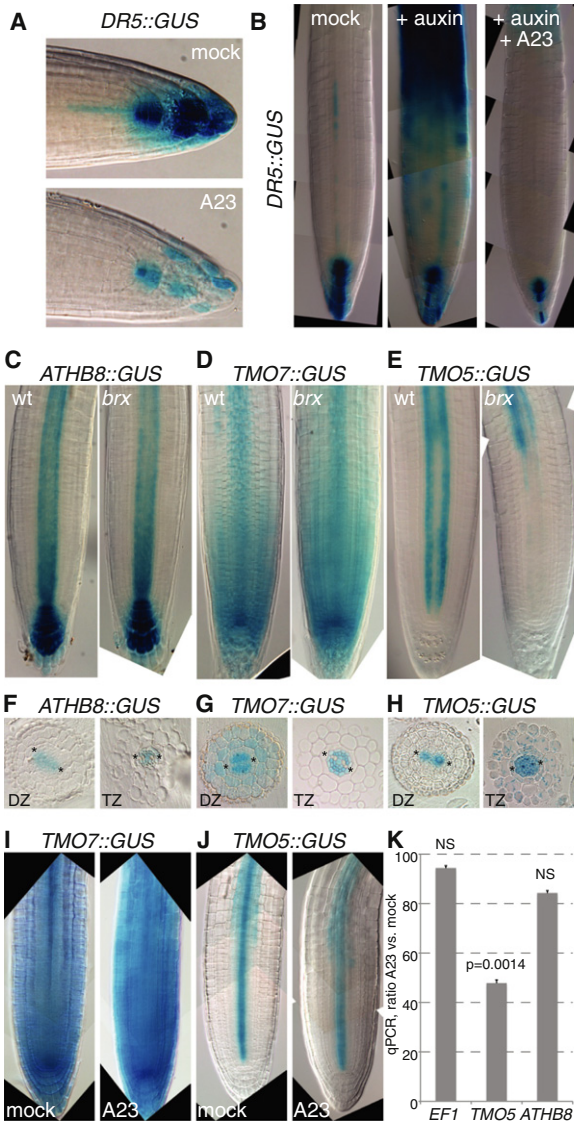

Figure 4. Endocytosis-Dependent Split of Auxin Response across the Transition Zone

(A) Reduced expression of the *DR5::GUS* marker upon A23 treatment (30 μM, 2 hr).

(B) Reduced *DR5::GUS* auxin response (10 μM indole-3-acetic acid treatment) in the transition zone upon parallel endocytosis block by tyrphostin A23 treatment (30 μM, 2hr).

(C–E) Expression levels and patterns of GUS reporter lines for confirmed auxin response factor (ARF) targets in wild-type (wt) and *brx* mutant. Note the drastic reduction of *TMO5* expression in *brx* specifically across the transition zone (E).

(F–H) Corresponding radial expression patterns visualized in 85 μm sections taken from the division (DZ) or transition (TZ) zones of individual roots. Xylem poles are indicated by asterisks.

(I and J) GUS staining patterns for the *TMO5* and *TMO7* reporters after mock or tyrphostin A23 treatment (30 μM, 30 min.) at 3 days after germination. Note that *TMO5::GUS* is oriented such that the protophloem plane is viewed, i.e., compared to Figure 1A or Figure 4E, only one protoxylem strand is visible.

(K) Ratio of transcript abundance between tyrphostin A23 treatment (30 μM, 30 min) and mock treatment as determined by qPCR (two technical replicates for each of three biological replicates, i.e., n = 6; 3-day-old roots) for *TMO5*, *ATHB8*, and the housekeeping gene elongation factor 1 (*EF1*). Error bars indicate standard errors; NS, not significant.

from the (vascular) transition zone onward, *TMO5* starts to be expressed throughout the vascular cylinder (Figure 4H; Figure S1F). Finally, consistent with its BRX and thus presumably endocytosis dependence, *TMO5* expression was significantly affected by tyrphostin A23 treatment, unlike *TMO7*, *ATHB8*, or a housekeeping gene (Figures 4I–4K).

In summary, the results from our combined experimental modeling approach support the idea that clathrin-mediated endocytosis directly influences auxin-responsive gene expression through regulation of nuclear BRX abundance. Because endocytosis activity is not uniform throughout the root meristem, this splits transcriptional auxin perception and sustains expression of selected genes across the division and transition zones to drive meristem growth. Thus, the endocytosis pattern provides positional information to interpret the auxin gradient, thereby extending the action spectrum of this hormonal cue.

Supplemental Information

Supplemental Information includes one figure, Supplemental Experimental Procedures, and three movies and can be found with this article online at doi:10.1016/j.cub.2011.10.002.

Acknowledgments

We would like to thank the Swiss Institute of Bioinformatics and the Lausanne Cellular Imaging Facility for technical support. This work was supported by Swiss National Science Foundation grant 31003A_129783 (C.S.H.), the SystemsX "Plant Growth in a Changing Environment" network (C.S.H. and R.S.S.), the BRAVISSIMO Marie Curie Initial Training Network (E.S.), and European Molecular Biology Organization long-term postdoctoral fellowships (A.R.-V. and E.M.N.D.).

Received: August 8, 2011
Revised: September 14, 2011
Accepted: October 4, 2011
Published online: November 10, 2011

References

1. Blilou, I., Xu, J., Wildwater, M., Willemsen, V., Paponov, I., Friml, J., Heidstra, R., Aida, M., Palme, K., and Scheres, B. (2005). The PIN auxin efflux facilitator network controls growth and patterning in Arabidopsis roots. Nature *433*, 39–44.
2. Petersson, S.V., Johansson, A.I., Kowalczyk, M., Makoveychuk, A., Wang, J.Y., Moritz, T., Grebe, M., Benfey, P.N., Sandberg, G., and Ljung, K. (2009). An auxin gradient and maximum in the Arabidopsis root apex shown by high-resolution cell-specific analysis of IAA distribution and synthesis. Plant Cell *21*, 1659–1668.
3. Sabatini, S., Beis, D., Wolkenfelt, H., Murfett, J., Guilfoyle, T., Malamy, J., Benfey, P., Leyser, O., Bechtold, N., Weisbeek, P., and Scheres, B. (1999). An auxin-dependent distal organizer of pattern and polarity in the Arabidopsis root. Cell *99*, 463–472.
4. Dello Ioio, R., Nakamura, K., Moubayidin, L., Perilli, S., Taniguchi, M., Morita, M.T., Aoyama, T., Costantino, P., and Sabatini, S. (2008). A genetic framework for the control of cell division and differentiation in the root meristem. Science *322*, 1380–1384.
5. Moubayidin, L., Perilli, S., Dello Ioio, R., Di Mambro, R., Costantino, P., and Sabatini, S. (2010). The rate of cell differentiation controls the Arabidopsis root meristem growth phase. Curr. Biol. *20*, 1138–1143.
6. Scacchi, E., Salinas, P., Gujas, B., Santuari, L., Krogan, N., Ragni, L., Berleth, T., and Hardtke, C.S. (2010). Spatio-temporal sequence of cross-regulatory events in root meristem growth. Proc. Natl. Acad. Sci. USA *107*, 22734–22739.
7. Mouchel, C.F., Osmont, K.S., and Hardtke, C.S. (2006). BRX mediates feedback between brassinosteroid levels and auxin signalling in root growth. Nature *443*, 458–461.
8. Truernit, E., Bauby, H., Dubreucq, B., Grandjean, O., Runions, J., Barthélémy, J., and Palauqui, J.C. (2008). High-resolution whole-mount imaging of three-dimensional tissue organization and gene expression

enables the study of Phloem development and structure in Arabidopsis. Plant Cell *20*, 1494–1503.

9. Grieneisen, V.A., Xu, J., Marée, A.F., Hogeweg, P., and Scheres, B. (2007). Auxin transport is sufficient to generate a maximum and gradient guiding root growth. Nature *449*, 1008–1013.
10. Vernoux, T., Brunoud, G., Farcot, E., Morin, V., Van den Daele, H., Legrand, J., Oliva, M., Das, P., Larrieu, A., Wells, D., et al. (2011). The auxin signalling network translates dynamic input into robust patterning at the shoot apex. Mol. Syst. Biol. *7*, 508.
11. Benjamins, R., and Scheres, B. (2008). Auxin: the looping star in plant development. Annu. Rev. Plant Biol. *59*, 443–465.
12. Dharmasiri, N., Dharmasiri, S., and Estelle, M. (2005). The F-box protein TIR1 is an auxin receptor. Nature *435*, 441–445.
13. Kepinski, S., and Leyser, O. (2005). The Arabidopsis F-box protein TIR1 is an auxin receptor. Nature *435*, 446–451.
14. Parry, G., Calderon-Villalobos, L.I., Prigge, M., Peret, B., Dharmasiri, S., Itoh, H., Lechner, E., Gray, W.M., Bennett, M., and Estelle, M. (2009). Complex regulation of the TIR1/AFB family of auxin receptors. Proc. Natl. Acad. Sci. USA *106*, 22540–22545.
15. Swarup, R., Friml, J., Marchant, A., Ljung, K., Sandberg, G., Palme, K., and Bennett, M. (2001). Localization of the auxin permease AUX1 suggests two functionally distinct hormone transport pathways operate in the Arabidopsis root apex. Genes Dev. *15*, 2648–2653.
16. Petrásek, J., and Friml, J. (2009). Auxin transport routes in plant development. Development *136*, 2675–2688.
17. Wisniewska, J., Xu, J., Seifertová, D., Brewer, P.B., Ruzicka, K., Blilou, I., Rouquié, D., Benková, E., Scheres, B., and Friml, J. (2006). Polar PIN localization directs auxin flow in plants. Science *312*, 883.
18. Mouchel, C.F., Briggs, G.C., and Hardtke, C.S. (2004). Natural genetic variation in Arabidopsis identifies BREVIS RADIX, a novel regulator of cell proliferation and elongation in the root. Genes Dev. *18*, 700–714.
19. Scacchi, E., Osmont, K.S., Beuchat, J., Salinas, P., Navarrete-Gómez, M., Trigueros, M., Ferrándiz, C., and Hardtke, C.S. (2009). Dynamic, auxin-responsive plasma membrane-to-nucleus movement of Arabidopsis BRX. Development *136*, 2059–2067.
20. Doherty, G.J., and McMahon, H.T. (2009). Mechanisms of endocytosis. Annu. Rev. Biochem. *78*, 857–902.
21. Robert, S., Kleine-Vehn, J., Barbez, E., Sauer, M., Paciorek, T., Baster, P., Vanneste, S., Zhang, J., Simon, S., Čovanová, M., et al. (2010). ABP1 mediates auxin inhibition of clathrin-dependent endocytosis in Arabidopsis. Cell *143*, 111–121.
22. Kramer, E.M. (2009). Auxin-regulated cell polarity: an inside job? Trends Plant Sci. *14*, 242–247.
23. Donner, T.J., Sherr, I., and Scarpella, E. (2009). Regulation of preprocambial cell state acquisition by auxin signaling in Arabidopsis leaves. Development *136*, 3235–3246.
24. Schlereth, A., Möller, B., Liu, W., Kientz, M., Flipse, J., Rademacher, E.H., Schmid, M., Jürgens, G., and Weijers, D. (2010). MONOPTEROS controls embryonic root initiation by regulating a mobile transcription factor. Nature *464*, 913–916.
25. Cutler, S.R., Ehrhardt, D.W., Griffitts, J.S., and Somerville, C.R. (2000). Random GFP:cDNA fusions enable visualization of subcellular structures in cells of Arabidopsis at a high frequency. Proc. Natl. Acad. Sci. USA *97*, 3718–3723.